Transverse particle dynamics in a Bessel beam

Graham Milne,[1] Kishan Dholakia,[1*] David McGloin,[2] Karen Volke-Sepulveda,[3] and Pavel Zemánek[4]

[1]*School of Physics and Astronomy,University of St Andrews, St Andrews, KY16 9SS, UK*
[2]*School of Engineering, Physics and Mathematics, University of Dundee, Dundee, DD1 4HN, UK*
[3]*Instituto de Física, Universidad Nacional Autónoma de México, Apdo. Postal 20-364, Mexico 01000*
[4]*Institute of Scientific Instruments of the ASCR, v.v.i. Academy of Sciences of the Czech Republic, Kralovopolska 147, 612 64 Brno, Czech Republic*
**Corresponding author: kd1@st-and.ac.uk*

Abstract: Spatially periodic optical fields can be used to sort dielectric microscopic particles as a function of size, shape or refractive index. In this paper we elucidate through both theory and experiment the behavior of silica microspheres moving under the influence of the periodic optical field provided by a Bessel beam. We compare two different computational models, one based on Mie scattering, the other on geometrical ray optics and find good qualitative agreement, with both models predicting the existence of distinct size-dependent phases of particle behavior. We verify these predictions by providing experimental observations of the individual behavioral phases.

OCIS codes: (350.4855) Optical tweezers or optical manipulation; (140.7010) Laser trapping; (140.3300) Laser beam shaping.

References and links

1. A. Ashkin, J.M. Dziedzic, J.E. Bjorkholm and S. Chu, "Observation of single-beam gradient force optical trap for dielectric particles," Opt. Lett. **11,** 288 (1986).
2. K. C. Neuman and S. M. Block, "Optical trapping," Rev. Sci. Instr. **75**, 2787 (2004).
3. C. Bustamante, Z. Bryan, and S. B. Smith,"Ten years of tension: single-molecule DNA mechanics," Nature **421,** 423 (2003).
4. K. Dholakia and P. Reece, "Optical micromanipulation takes hold," Nano Today **1**, 18 (2006).
5. MJ. Enger, M. Goksör, K. Ramser, P. Hagberg and D.Hanstorp, "Optical tweezers applied to a microfluidic system," Lab on a Chip **4,** 196 – 200 (2004).
6. P. T. Korda, . C. Spalding and D.G. Grier, "Evolution of a colloidal critical state in an optical pinning potential landscape," Phys. Rev. B **66,** 024504 (2002).
7. M.P. MacDonald, G.C. Spalding and K. Dholakia, "Microfluidic sorting in an optical lattice," Nature **426,** 421 (2003).
8. M. Pelton, K. Ladavac and D. G. Grier, "Transport and fractionation in periodic potential-energy landscapes," Phys. Rev. E **70,** 031108 (2004).
9. I. Ricárdez-Vargas, P. Rodríguez-Montero, R. Ramos-García and K. Volke-Sepúlveda, "A modulated optical sieve for sorting of polydisperse microparticles," Appl. Phys. Lett. **88,** 121116 (2006).
10. T. Cizmar, M. Siler, M. Sery, P. Zemanek, V. Garcés-Chávez, and K. Dholakia, "Optical sorting and detection of submicrometer objects in a motional standing wave," Phys. Rev. B **74,** 035105 (2006).
11. S. Lee and D. G. Grier, "One-dimensional optical thermal ratchets," J. Phys.: Condensed Matter **17,** S3685-S3695 (2006).
12. L. McCann, M.I. Dykman, and B. Golding, "Thermally activated transitions in a bistable three-dimensional optical trap," Nature **402,** 785 (1999).
13. P. Zemanek, A. Jonas, and M. Liska, "Simplified description of optical forces acting on a nanoparticle in the Gaussian standing wave," J. Opt. Soc. Am. A **19,** 1025 (2002).
14. P. Jakl, M. Sery, J. Jezek, A. Jonas, M. Liska, and P. Zemanek,"Behaviour of an optically trapped probe approaching a dielectric interface," J. Mod. Opt. **50,** 1615 (2003).
15. T. Cizmar, V. Garcés-Chávez, K. Dholakia, P. Zemanek, "Optical conveyor belt for delivery of submicron objects", Appl. Phys. Lett. **86,** 174101 (2005).
16. T. Cizmar, V. Kollarova, Z. Bouchal, and P. Zemanek,"Sub-micron particle organization by self-imaging of non-diffracting beams," New J. Phys. **8,** 43 (2006).

#86741 - $15.00 USD Received 21 Aug 2007; revised 2 Oct 2007; accepted 3 Oct 2007; published 9 Oct 2007

17. S. A. Tatarkova, W. Sibbett and K. Dholakia, "Brownian particle in an optical potential of the washboard type," Phys. Rev. Lett. **91**, 038101 (2003).
18. L. Paterson, E. Papagiakoumou, G. Milne, V. Garcés-Chávez, S. A. Tatarkova, W. Sibbett, F. J. Gunn-Moore, P. E. Bryant, A.C. Riches and K. Dholakia, "Light-induced cell separation in a tailored optical landscape," Appl. Phys. Lett. **87,** 123901 (2005).
19. K. Volke-Sepulveda, S. Chávez-Cerda, V. Garcés-Chávez and K. Dholakia, "Three-dimensional optical forces and transfer of orbital angular momentum from multi-ringed light beams to spherical microparticles," J. Opt. Soc. Am. B **21**, 1749 (2004).
20. J. Durnin, "Exact solutions for diffracting beams. I. The scalar theory," J. Opt. Soc. Am. A **4,** 651 (1987).
21. D. McGloin and K. Dholakia, "Bessel Beams: Diffraction in a new light," Contemp. Phys. **46,** 15 (2005).
22. J. Arlt, K. Dholakia, J. Soneson, and E. M. Wright, "Optical dipole traps and atomic waveguides based on Bessel light beams," Phys. Rev. A **63,** 063602 (2001).
23. D. McGloin, G.C. Spalding, H. Melville, W. Sibbett and K. Dholakia, "Three-dimensional arrays of optical bottle beams," Opt. Comm. **225,** 215 (2003).
24. K. Visscher and G.J. Brakenhoff, A theoretical study of optically induced forces on spherical particles in a single beam trap I: Rayleigh scatterers. Optik **89,** 174 (1992).
25. P. C. Chaumet and M. Nieto-Vesperinas, "Time-averaged total force on a dipolar sphere in an electromagnetic field," Opt. Lett. **25,** 1085 (2000).
26. J. P. Barton, D. R. Alexander, and S. A. Schaub, "Theoretical determination of net radiation force and torque for a spherical particle illuminated by a focused laser beam," J. Appl. Phys. **66,** 4594 (1989).
27. V. Garcés-Chávez, K. Volke-Sepúlveda, S. Chávez-Cerda, W. Sibbett and K. Dholakia, "Transfer of orbital angular momentum to an optically trapped low-index particle," Phys. Rev. A **66,** 063402 (2002).
28. R. Gussgard, T. Lindmo, and I. Brevik, "Calculation of the trapping force in a strongly focused laser beam," J. Opt. Soc. Am. B **9,** 1922 (1992).
29. G. Milne, "St Andrews Tracker," http://faculty.washington.edu/gmilne/tracker.htm.
30. N. Chattrapiban, E.A. Rogers, D. Cofield, W.T. Hill, and R. Roy, "Generation of nondiffracting bessel beams by use of a spatial light modulator," Opt. Lett. **28,** 2183 (2003).

1. Introduction

It is now well known that focused light beams can be used to trap and manipulate microscopic particles [1]. Optical tweezers, as this technique has become known, have enabled key advances in many branches of science. In biology they provide an ideal tool for the study of molecular motors and DNA at the single-molecule level [2,3]. In the physical sciences optical tweezers have also enabled a wide range of studies in colloid science, optical angular momentum and microfluidics [4,5]. Stationary extended patterns of light (also termed *optical landscapes*) have been used to arrange and accumulate microparticles in pre-described arrays [6]. More recent work has shown that optical lattices may be used to separate biological material in a microfluidic flow, due to the varying response of the particles to the underlying optical potential energy landscape (a function of their size, shape and relative refractive index) [7,8]. The interactions of particles with time-varying optical landscapes have also been studied in the context of particle sorting [9,10] and thermal ratchets [11].

Several authors have already discussed the relationship between the Brownian motion of microscopic particles and applied optical fields. McCann *et al.* [12] showed that Kramers' theory for the thermally activated escape from a potential well could be used to describe the movement of 0.6μm silica particles between two overlapping optical traps. The behavior of spherical objects in a one-dimensional periodic optical landscape has been studied in detail both theoretically and experimentally by Zemanek *et al.* [13-16] and a strong dependence of the optical force on particle size has been proved. Tatarkova *et al.* [17] showed that Brownian motion could be combined with the one-dimensional optical potential provided laterally by the rings of a single *tilted* Bessel beam (a *washboard potential*) to produce directed Brownian transport of microscopic particles. It has been observed that for biological samples, where typical particle length scales are larger than the ring spacing, there is no need for the tilting of the intensity profile of the Bessel beam in order to activate particle motion [18]. In general, these studies have provided solid experimental evidence of a strong dependence of the

#86741 - $15.00 USD Received 21 Aug 2007; revised 2 Oct 2007; accepted 3 Oct 2007; published 9 Oct 2007

interactions between light and microscopic particles on the geometry of the particles and their relative size with respect to the characteristic dimensions of the optical landscape.

Theoretical calculations for the optical forces in different potential landscapes support some of the experimental observations that have been reported [13,15,19]. Although equilibrium positions can be established by considering the forces alone, a simultaneous examination of the associated potential energy profile can help to elucidate key aspects of the overall particle behavior within the optical distribution

In this paper, we examine in detail the dynamics of particles moving under the influence of the optical landscape associated with the transverse cross-section of a Bessel beam. The azimuthally-symmetric nature of this profile implies that we can consider the particles as moving in a one-dimensional (radial) potential. As we discuss the motion of particles in a horizontal plane, both gravity and the radiation pressure force along the direction of beam propagation can be neglected and the coupling of thermal forces with the optical field becomes the main consideration.

We compare experimental observations with theoretical predictions for the optical forces and potentials calculated by means of two alternative approaches. We believe this study will provide a backdrop for the design of *ad hoc* tailored optical landscapes that may give rise to several potential applications, particularly with relation to optical sorting.

2. Optical forces and potentials: theoretical modeling

For our case study, we will consider the light intensity distribution associated with a zeroth-order Bessel beam. For a recent review of Bessel beams and their potential applications, see [20]. Bessel beams were first introduced by Durnin [21] as propagation-invariant or diffraction-free optical fields. We can think of the wave vectors **k** of the plane waves that combine to form a Bessel beam as lying on the surface of a cone. The apex angle α of this imaginary cone provides us with the expressions $k_r=k\sin(\alpha)$ and $k_z=k\cos(\alpha)$ for the radial and axial components of the wave vectors. The electric component of the optical field of an ideal zeroth-order Bessel beam is given in the paraxial approximation by

$$E(\mathbf{r},t) = E_{0B} J_0(k_r r)\exp\left\{i\left(k_z z - \omega t\right)\right\}, \tag{1}$$

where E_{0B} is the amplitude of the electric field on the optical axis of the Bessel beam, J_0 is the first class Bessel function of zeroth-order and ω is the angular frequency of the field. Experimentally, a reasonable and efficient approximation to an ideal Bessel beam can be generated within a finite region of space by illuminating a conical lens – also called an *axicon* – with a well-collimated Gaussian beam. The distance over which this Bessel beam can be considered non-diffracting (Fig. 1(a)) is commonly known as the *maximum propagation distance* and is denoted by z_{max}. The corresponding intensity distribution can be approximated using the stationary phase method to yield [22]

$$I(r,z) = \frac{4k_r P}{w_c}\frac{z}{z_{\max}} J_0^2(k_r r)\exp\left\{-\frac{2z^2}{z_{\max}^2}\right\}. \tag{2}$$

Here P represents the power of the incident Gaussian beam, while w_c is the beam's half-width. The maximum propagation distance z_{max} can be expressed as:

$$z_{\max} = \frac{w_c}{\tan(\alpha)}, \tag{3}$$

where for small α, $\alpha \approx (n_{ax}\text{-}1)\gamma$ in air and $z_{max}\approx w_c/[(n_{ax}\text{-}1)\gamma]$. n_{ax} is the refractive index of the axicon and γ is its opening angle.

In cross-section (Fig. 1(b)), this beam is characterized by a bright core surrounded by concentric rings of decreasing intensity. From the term $J_0(k_r r)$ in Eq. (2) the characteristic

#86741 - $15.00 USD Received 21 Aug 2007; revised 2 Oct 2007; accepted 3 Oct 2007; published 9 Oct 2007

transverse dimensions of the beam depend on k_r and consequently on the axicon parameter γ. In practice a system of lenses can be added after the axicon to reduce the ring structure to a scale appropriate for optical micro-manipulation. We define the width of a particular ring as the distance between two consecutive radial intensity minima. Theoretically, the width of the n-th Bessel beam ring is given by $\Delta\rho_n = (\Delta x_n/k_r)$, where $\Delta x_n = (x_{n+1} - x_n)$ represents the separation between two consecutive roots in the zero-order Bessel function. As $n\rightarrow\infty$, Δx_n quickly converges to π and we can approximate

$$\Delta\rho \approx \frac{\lambda}{2\sin\alpha}, \tag{4}$$

where λ is the wavelength in the medium in which the Bessel beam is formed.

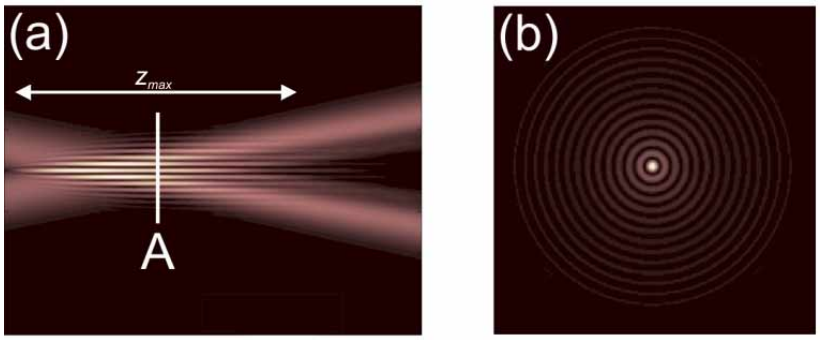

Fig. 1. (Color online) (a) Cross-section of a Bessel beam along direction of propagation. (b) Cross-section perpendicular to direction of propagation, taken at point A in (a). The figures were generated using a fast Fourier transform beam propagation algorithm, as used in previous work [23].

In this paper we are primarily concerned with the properties of Bessel beams in the transverse plane. For this reason, in our calculations we set a fixed z plane at the position of maximum intensity along the beam propagation axis. From Eq. (2) this position is given by $z_{peak}=z_{max}/2$. It is important to note that because the Bessel beam does not change significantly over small displacements along the direction of propagation, slight movement of a microscopic particle along z will not cause significant variations in the associated optical potential. This is not the case with conventional optical traps [1,12].

Given a light intensity distribution, optical forces and potentials can be calculated by using different approximations, depending on the particle's radius, R_0, with respect to the wavelength λ of the light in the medium. In the Rayleigh regime ($R_0<<\lambda$), the particles are implicitly very small and can be approximated as point dipoles. In this case the shape of the optical force and potential energy distributions as a function of the particle's position turns out to be independent of the particle size or geometry, and depends only on the light distribution itself [24,25]. In contrast, for larger spherical objects, where $R_0\approx\lambda$ or $R_0>>\lambda$, forces can be calculated by a rigorous electromagnetic model based on Mie scattering theory [16,26] or by ray-tracing methods [19,27,28].

In this paper we present calculations obtained using the Mie scattering theory and compare the findings with experimental observations. We also performed calculations using a simpler geometric ray optics model, and towards the end of the paper provide a qualitative comparison of the two models.

Our primary method for optical force calculation is based on light scattering and it assumes that the beam created behind the axicon possesses the form of an ideal non-

#86741 - $15.00 USD Received 21 Aug 2007; revised 2 Oct 2007; accepted 3 Oct 2007; published 9 Oct 2007

diffracting beam that does not change its properties upon propagation. This is a vectorial expression and is also valid for non-paraxial configurations. The following form of the electric and magnetic components of the field has been found [16,26]:

$$\mathbf{E}(r,\phi,z) = E_{B0}\exp(ik_z z)\Big\{\Big[\,J_0(k_r r) + J_2(k_r r)\beta^2\cos(2\phi)\,\Big]\mathbf{e}_x + J_2(k_r r)\beta^2\sin(2\phi)\mathbf{e}_y - i2J_1(k_r r)\beta\cos(\phi)\mathbf{e}_z\,\Big\}, \tag{5}$$

$$\mathbf{B}(r,\phi,z) = \frac{k}{\omega}E_{B0}\exp(ik_z z)\Big\{\,J_2(k_r r)\beta^2\sin(2\phi)\mathbf{e}_x + \Big[\,J_0(k_r r) - J_2(k_r r)\beta^2\cos(2\phi)\,\Big]\mathbf{e}_y - i2J_1(k_r r)\beta\sin(\phi)\mathbf{e}_z\,\Big\}, \tag{6}$$

where $\mathbf{e}_{x,y,z}$ are the cartesian unit vectors and ϕ is the azimuthal angle in the beam-centred cylindrical system of coordinates ($\phi = 0$ implies that the x-axis is aligned along the direction of the linear polarization of the beam incident on the axicon). E_{B0} is the electric field amplitude of this non-diffracting beam on the optical axis and J_m is the first class Bessel function of mth order. The parameter $\beta = \sin\alpha/(1+\cos\alpha)$ is responsible for an asymmetry in this non-diffracting beam which becomes more significant as the angle α increases. In the limit $\beta \to 0$, we obtain a scalar electric field that has the same spatial transversal profile as the Bessel beam considered in Eq. (1).

Given a vectorial description of the beam, the optical force calculations based on the Mie theory require a decomposition of the incident beam into a system of spherical harmonics with amplitudes

$$A_{lm} = \frac{1}{l(l+1)\psi_l(\xi)}\int_0^{2\pi}\int_0^{\pi}\sin\theta E_r^i(r_0,z_0)Y_{lm}^*(\theta,\varphi)d\theta d\varphi, \tag{7}$$

$$B_{lm} = \frac{1}{l(l+1)\psi_l(\xi)}\int_0^{2\pi}\int_0^{\pi}\sin\theta B_r^i(r_0,z_0)Y_{lm}^*(\theta,\varphi)d\theta d\varphi, \tag{8}$$

where $\xi = 2\pi R_0/\lambda$, E_r^i and B_r^i are the radial components of the electric and magnetic fields respectively, incident on the surface of the spherical particle (expressed in spherical coordinates as (R_0, φ, θ) with the origin at the sphere centre), Y_{lm}^* are the complex-conjugated spherical harmonics and ψ is the Ricatti-Bessel function. In this description the beam is not strictly azimuthally symmetrical and

$$r_0 = \sqrt{r^2 + R_0^2\sin^2\theta + 2R_0 r\cos(\varphi-\varphi_0)\sin\theta}, \qquad z_0 = z + R_0\cos\theta \tag{9}$$

where φ_0 is the azimuthal angle of the centre of the sphere in the cylindrical system of coordinates of the beam. The forces and torques acting on a spherical object can be calculated from the equations presented by Barton [26].

Computationally, the double integration in Eqs. (7) and (8) can be time consuming. By applying the idealized non-diffracting properties of this beam formed behind the axicon, we simplify the coefficients A_{lm} and B_{lm} and require only a single integration [16]. Despite this simplification, this approach is still computationally demanding. Computation time increases with particle size and for spheres much larger than a micron it may be preferable to turn to a simpler, geometrical model if computation time is a concern.

#86741 - $15.00 USD Received 21 Aug 2007; revised 2 Oct 2007; accepted 3 Oct 2007; published 9 Oct 2007

To calculate the transverse optical force in the ray optics regime, we employ a model developed in previous work [19,27]. In this case our zeroth-order Bessel beam is considered to be an azimuthally symmetric intensity distribution for which the energy flux is directed only along the beam axis (z). The basic equation for obtaining the radial optical force exerted on a dielectric sphere of radius R_0 can be written as

$$F_\rho(r,z)=\frac{n_m R_0^2}{2c}\int_0^{\pi/2}\int_0^{2\pi} I(r_0,z_0)\left[R\sin 2\theta - T^2\left(\frac{\sin 2(\theta-\theta_t)+R\sin 2\theta}{1+R^2+2R\cos 2\theta_t}\right)\right]\sin 2\theta\cos\varphi\, d\varphi\, d\theta. \tag{10}$$

The integration is carried out over the illuminated hemisphere of the particle $\theta\in[0,\pi]$, $\varphi\in[0,2\pi]$; where θ and φ are the polar and azimuthal angles, respectively, in spherical coordinates. As we have assumed that all of the light rays arrive parallel to beam axis, θ coincides with the incidence angle at each point on the sphere's surface and the transmitted angle is denoted by θ_t. R and T represent the reflectance and transmittance coefficients averaged over the two transverse polarization directions at each point and c/n_m represents the speed of light in the surrounding medium. We use Eq. (2) here to describe the intensity of the incident beam.

The coordinates of each point at the particle's surface, (R_0, φ, θ), and the position of the particle's center within the beam profile, (r, z), are again related through Eq. (9), with $\varphi_0=0$ in this case since with this approach the beam is considered to be rotationally symmetric.

The external work needed to shift the particle radially from the beam center to some distance r is independent of the azimuthal coordinate and is defined as

$$U(r,z=z_{peak})=-\int_0^r F_\rho(r',z=z_{peak})\,dr'. \tag{11}$$

3. Experimental set-up

In order to monitor the behavior of different particles within a Bessel beam we implemented the experimental set-up illustrated in Fig. 2. The beam from a 1070nm fiber laser (IPG Laser), with a spot diameter of 1.6 mm, illuminated the back flat side of an axicon of angle $\gamma=1^\circ$. A pair of lenses reduced the dimensions of the Bessel beam so that the typical transverse ring thickness was of the order of the diameter of the particles under examination. Great care was taken to ensure that the intensity distribution was azimuthally invariant. A dielectric mirror directed the beam into the sample chamber while allowing white light back illumination to enter the system. A half-wave plate and polarizing beam-splitting cube allowed precise control over the power of the beam without altering the operating characteristics of the laser. The sample plane was imaged and observed by means of a 100x oil-immersion objective and a Pulnix PE2015 CCD camera. A second dielectric mirror diverted most of the Bessel beam away from the camera, transmitting only a small portion of the beam through onto the camera surface. The video signal was fed into a computer via a National Instruments IMAQ PCI-1408 video capture card and stored for subsequent analysis. A single-beam optical trap was also incorporated into the set-up in order to allow precise and consistent positioning of individual particles at predetermined regions of interest within the Bessel beam profile. For this purpose, part of the output laser beam was diverted before the axicon and redirected through the back aperture of the imaging objective. A system of mirrors and lenses made the optical tweezers fully steerable in the sample plane. Following particle placement at a specific location within the Bessel beam, the tweezers beam was blocked, allowing the natural evolution of particle motion in the Bessel landscape to be monitored. Silica spheres with mean radii of $R_0=1.15\pm0.12\mu m$, $R_0=2.5\pm0.21\mu m$ and $R_0=3.42\pm0.29\mu m$ (Bangs Laboratories) were suspended in deuterium oxide (D_2O). D_2O was used instead of H_2O to minimize the effect of heating due to absorption of laser light at the wavelength of 1070nm. We did not consider

#86741 - $15.00 USD Received 21 Aug 2007; revised 2 Oct 2007; accepted 3 Oct 2007; published 9 Oct 2007

spheres smaller than 2.3μm because their more pronounced Brownian motion and tendency to diffuse away from the substrate made them difficult to follow using video tracking. Dilute colloidal samples were used to avoid any unwanted colloid-colloid interactions. The silica particles were denser than the surrounding medium and settled quickly to the bottom of the sample cell. The Bessel beam illuminated the sample from below. Elevation can occur when the particles reach the core [18] but the radiation pressure in the surrounding rings was not sufficient to raise the particles there away from the substrate. Trajectories of the particles were established by analyzing the output of the CCD camera with pattern-matching based particle-tracking software, which we developed specifically for this purpose [29].

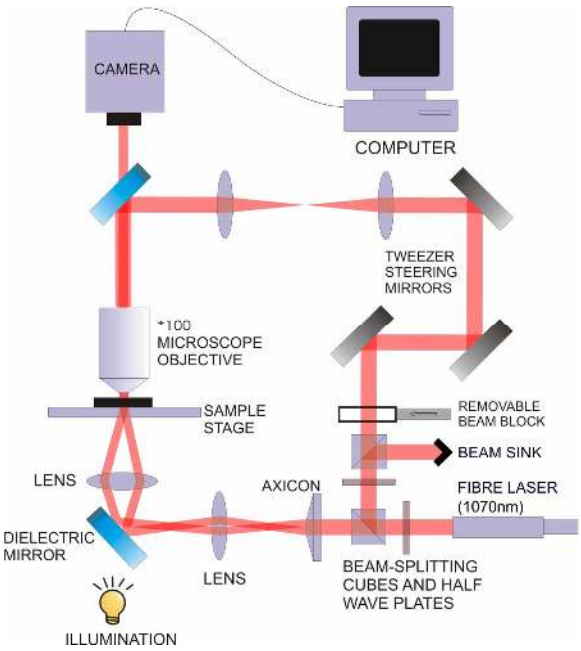

Fig. 2. (Color online) Overview of the experimental set-up. A system of beam cubes and half-wave plates modulated the power of a collimated 1070nm laser beam. One beam line illuminated an axicon, creating a Bessel beam, which was then imaged onto the sample stage. A second beam line was used to create a standard optical trap, with a 4f lens system mapping a steering mirror to the back aperture of the imaging microscope objective. A CCD camera was used to record particle behavior in the Bessel beam.

4. Results and discussion

In this section we present theoretical results predicting the optical forces and associated optical potentials obtained with the Mie model for four different particle sizes. On this basis, we realize a qualitative, comparative analysis with experimental observations of the equilibrium positions of the particles and their motion within the transversal Bessel optical landscape.

4.1 Theoretical results

The radial optical force and potential profiles were calculated for silica spheres of varying size. The complete set of results can be seen in the movie associated with Fig. 3. The shape of the potential energy landscape is strongly dependent on the sphere size. As the size is increased, distinct phases of particle behavior are observed.

#86741 - $15.00 USD Received 21 Aug 2007; revised 2 Oct 2007; accepted 3 Oct 2007; published 9 Oct 2007

The first distinctive phase of behavior concerns particles whose diameter is smaller than the characteristic ring width. As an example we consider a particle of radius R_0=1.15μm (Fig. 3) and a Bessel beam with a characteristic ring width of $\Delta\rho$=3.1μm. Equilibrium points are represented in the Fig. 3. by circles and correspond closely to local intensity maxima (the dashed curve represents the transverse radial intensity profile.)

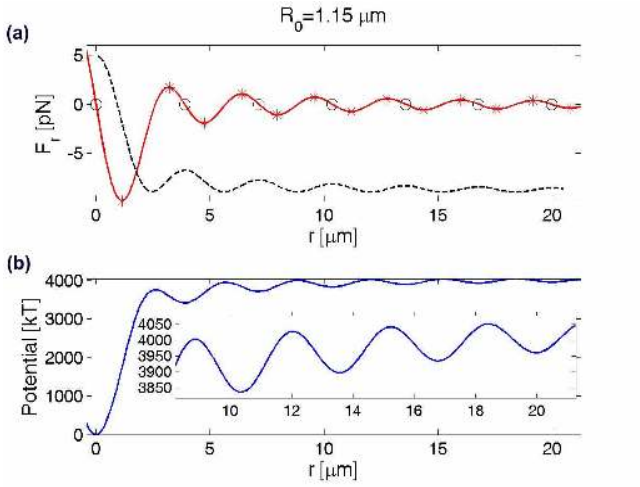

Fig. 3. [1.6MB] (Color online) Optical radial forces (red) and corresponding potential profiles (blue) obtained for a silica sphere of radius 1.15μm (refractive index n_b=1.4496) immersed in water (n_m=1.333) using the Mie scattering theory. The intensity of the Bessel beam on-axis was equal to the intensity obtained from Eq. (2) for $z=z_{max}/2$, P=200mW, $\lambda=1070/n_m$ nm, w_c=28.3μm, α=7.5°. The dashed curve shows the corresponding radial intensity profile of the Bessel beam. Circles denote the radial equilibrium positions, while * mark the extreme values of the optical force. The corresponding movie shows the dependency on particle radius.

Interestingly, although the Bessel beam itself is *untilted*, we still observe a washboard-like potential, with potential energy barriers lower on the inner side of each well (Fig. 3(b), inset). While we would expect small particles to remain radially localized at the potential energy minima, thermally activated escape from the well remains a possibility. Due to the lowering of the potential barriers on the inner side of each well, we expect to see particles move preferentially towards the beam core.

As we increase the particle size, we observe a change in behavior. As an example, for silica spheres with a radius R_0=2.15μm (Fig. 4(a, b)), the positive radial force regimes and corresponding potential energy barriers seen in Fig. 3 disappear. These particles are free to drift into the core of the Bessel beam without obstruction. This phenomenon is similar to the observed behavior of spheres in spatially periodic fields (standing waves) where spheres of a certain size do not feel the periodic field structure [9,10,13,15].

#86741 - $15.00 USD Received 21 Aug 2007; revised 2 Oct 2007; accepted 3 Oct 2007; published 9 Oct 2007

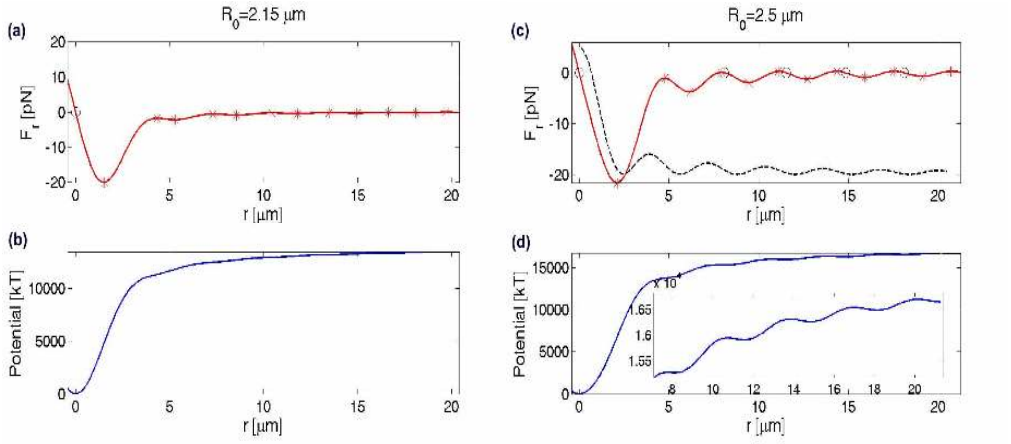

Fig. 4. (Color online) Optical radial forces (red) and corresponding potential energy profiles (blue) obtained for two sizes of silica spheres. From (a) we can see that when R_0=2.15μm the radial force is uniformly negative. The potential profile (b) shows only one equilibrium point, at the beam core. In contrast, increasing the particle size slightly to R_0=2.5μm (c) reveals a new regime where particles can be trapped radially in equilibrium points located between the rings (d). The dashed curve shows the corresponding radial intensity profile.

Increasing the sphere size slightly further reveals another regime, where particles can be radially trapped as they straddle two rings. As an example, Fig. 4(c, d) shows calculated plots for a sphere of radius R_0=2.5μm. The potential energy wells associated with this phenomenon (Fig. 4(d), inset) are significantly shallower than those associated with the R_0=1.15μm sphere (Fig. 3(b), inset). For example, at a radial position of r=10.4μm, we predict the R_0=1.15μm sphere to experience a potential well with a depth of 166kT. The R_0=2.5μm sphere, on the other hand, will experience a well at r=11.6μm with a depth of 34kT, almost five times shallower.

There exists a fourth and final distinct behavioral phase. Intuitively, since the core of a Bessel beam is considerably brighter than the surrounding rings, it might be expected that the center of the beam's core would coincide with the location of the bottom of the deepest potential well. For most particle sizes this is the case. For some sphere radii, however, core equilibrium positions exist which are not located at the centre of the beam but are displaced off-axis. Figure 5 shows the calculated radial force and potential profiles for a sphere of radius R_0=3.42μm. In this case the core equilibrium position of the sphere is offset from the beam core by 1.16μm. This behavior is highlighted in Fig. 6 and in the associated movie. Similar effects have been observed both theoretically and experimentally in spatially periodic fields [9,10,13,15].

#86741 - $15.00 USD Received 21 Aug 2007; revised 2 Oct 2007; accepted 3 Oct 2007; published 9 Oct 2007

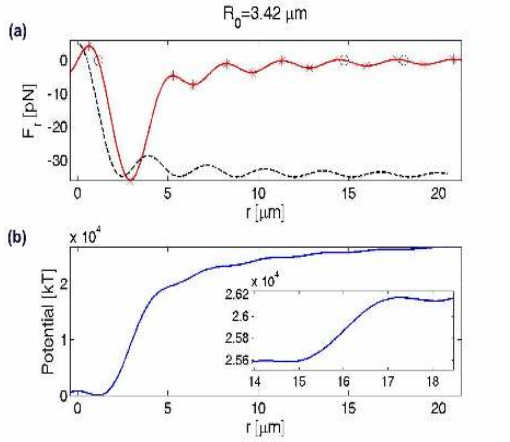

Fig. 5. (Color online) Optical radial forces (red) and corresponding potential profiles (blue) obtained for silica spheres of radius 3.42μm. The core equilibrium position is offset from the centre of the Bessel beam by approximately 1μm. Additionally, shallow potential energy wells can be seen 15μm and 18μm from the core (inset).

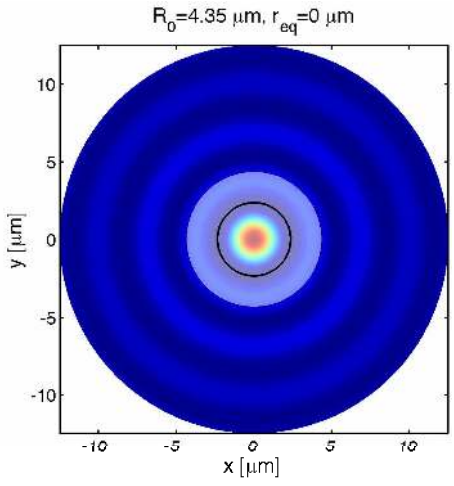

nm

Fig. 6. [1.5MB] (Color online) Transversal intensity profile of the Bessel beam with the equilibrium position of two selected spheres. The black ring (radius 2.35μm) denotes the first intensity minimum of the Bessel beam. The stable equilibrium point for the smaller particle (a) is localized off axis, while for the larger particle (b) it is aligned with the core of the Bessel beam. The associated movie shows the movement of the core equilibrium position as particle radius is increased.

4.2 Comparison with experiment

In this section we compare the behavior predicted by our Mie theory with experimental observations. From Fig. 3 it can be seen that for particles whose diameter is smaller than the typical ring spacing (R_0=1.15μm), positive radial force regimes exist across the profile. Stable equilibrium points exist at the roots of the force plot where the slope of the curve is negative. As expected, these positions correspond to local minima in the radial potential energy plot. For these minima, the height of the inner potential energy barrier (towards the beam core) is lower than the outer barrier. Under these circumstances, the particle behaves as it would in a tilted washboard potential [17] – there is higher probability of a thermally activated transition

#86741 - $15.00 USD Received 21 Aug 2007; revised 2 Oct 2007; accepted 3 Oct 2007; published 9 Oct 2007

towards the core of the beam than away from it. We therefore expect that a particle should, via a series of jumps both towards and away from the core, ultimately drift radially inwards.

In agreement with predictions from Fig. 3 we observed that when the power in the Bessel beam is sufficiently low the particles occasionally *hop* from one adjacent ring to another. We verified this behavior by recording the transitions of a particle between adjacent rings. A trajectory typical of a R_0=1.15μm particle is illustrated in Fig. 7. The particles are confined in the radial direction, but are free to move azimuthally around the rings. This image shows two consecutive hops from the fifth ring to the third ring. The hopping events occur swiftly and are easily identifiable.

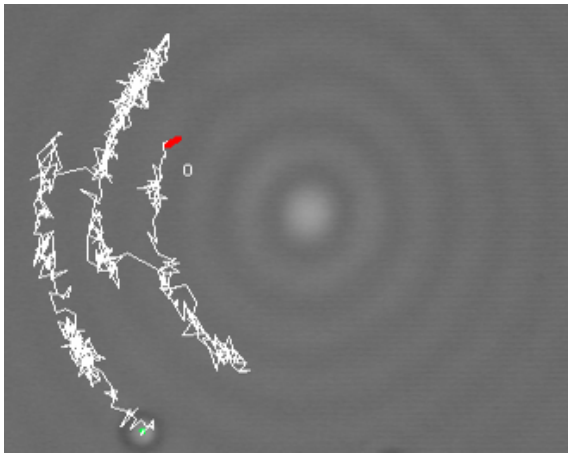

Fig. 7. Typical transversal trajectory of a R_0=1.15μm silica sphere in a Bessel beam. When a sphere escapes a ring, its transition to the adjacent ring is relatively direct.

The single beam optical trap was used to locate a R_0=1.15μm sphere at a precise point in the centre of the fifth ring. Blocking the tweezers beam released the particle and initiated a timer. Using the same sphere, 200 transition times were measured for four different Bessel beam power levels.

Figure 8 shows histograms of the transition times from the fifth ring at four different beam powers. In all cases the number of transitions inwards (green) is larger than the number of transitions outwards (red), in agreement with what we would expect from the theory. At powers greater than 200mW the transition times became so large that the collection of large data sets became impractical.

#86741 - $15.00 USD Received 21 Aug 2007; revised 2 Oct 2007; accepted 3 Oct 2007; published 9 Oct 2007

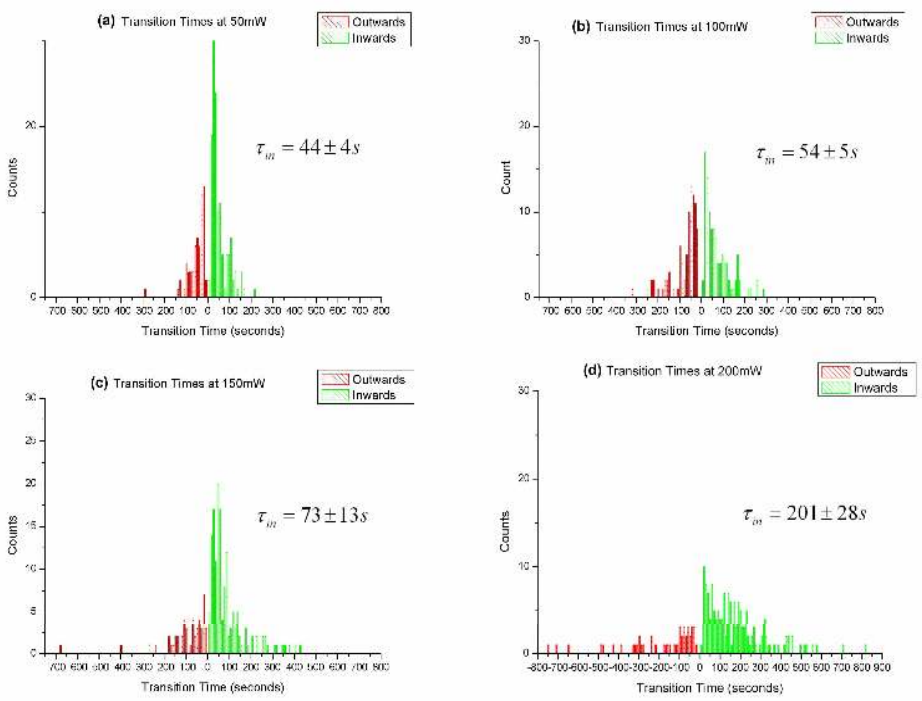

Fig. 8. (Color online) Histograms for the transition times of a R_0=1.15μm sphere from the 5th-ring of a Bessel beam for different values of the overall beam power: (a) 50mW, (b) 100mW, (c) 150mW, (d) 200mW. The mean escape time increases as the beam power is increased. Histograms have bin widths of 10secs. Red bars represent hops outwards, green represent hops inwards towards beam core. In each case τin represents the estimated mean first passage time, in seconds, towards the core of the beam.

Increasing the overall beam power results in a deepening of the potential wells, thereby increasing the mean escape time from a given ring. This is manifested in Fig. 8 as a broadening of the distributions for higher powers. We estimated the mean first passage time towards the core, τin. by fitting curves of the form $(1/\tau)\exp(-t/\tau)$ to the histograms. We see that the mean first passage time increases with increasing beam power, as we might expect.

For the case of R_0=2.5μm, we observed that, as predicted, equilibrium positions exist in a configuration whereby the particle straddles two of the rings. At distances less than 8μm from the core our model predicts no stable equilibrium points and we observed experimentally that in this range the particle does indeed travel into the core of the beam uninhibited. This can be seen in Fig. 9(a), which represents a 21-second video sequence. The particle is briefly localized between the 2nd and 3rd rings (r≈8μm), which agrees well with our prediction of the presence of a shallow potential well at this location.

At radial distances larger than 8μm, further small positive force regimes can be seen (Fig. 4(c)). In contrast to the case of the R_0=1.15μm particle, the potential energy minima for R_0=2.5μm correspond spatially to local intensity *minima* of the beam profile. This scenario is similar to the case of spheres placed in a one-dimensional tilted standing wave, with all the consequences [13,14]. Fig. 9(b) shows a 2.5μm particle moving in the region between the fifth and sixth rings. As the potential wells at this distance are relatively broad and shallow (Fig. 4(d), inset), the particle exhibits some degree of freedom, however the Kramers' time for the escape of a particle from a potential well scales with the fluid drag and we find that the larger 2.5μm spheres can be trapped in these states for a comparatively long time. This trajectory

#86741 - $15.00 USD Received 21 Aug 2007; revised 2 Oct 2007; accepted 3 Oct 2007; published 9 Oct 2007

represents movement over 1000 seconds of video, considerably longer than the typical ring occupation time of R_0=1.15µm spheres at a similar radial distance and overall beam power.

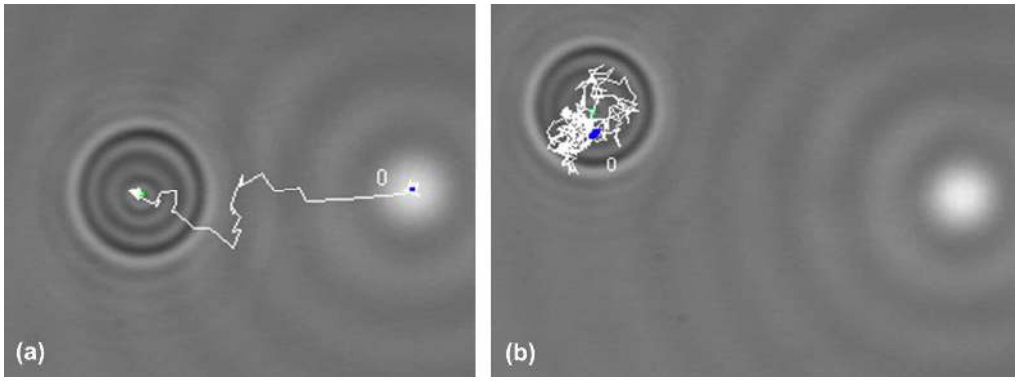

Fig. 9. (Color online) (a) A typical trajectory for a R_0=2.5µm silica particle in a Bessel beam closer to the core. (b) Away from the core, R_0=2.5µm particles can be trapped loosely across two rings. Beam power is 200mW in both cases.

Our Mie model predicts that for a particle of radius R_0=3.42µm, the core equilibrium position will be offset from the centre of the beam by 1.15µm (Fig. 5). The offset equilibrium position has been observed experimentally with excellent agreement and a typical particle trajectory can be seen in Fig. 10. The mean radial core separation distance for this stably trapped particle is ~1µm.

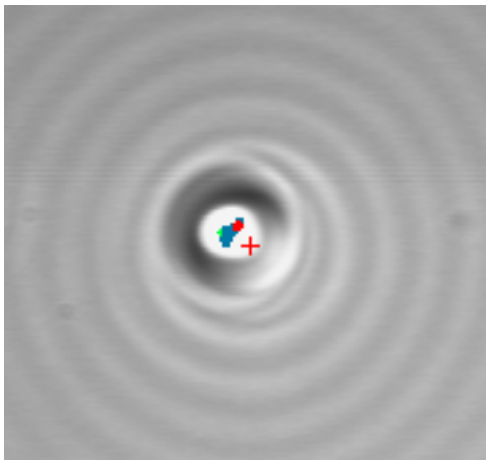

Fig. 10. (Color online) A with R_0=3.42µm particle has been tracked for over 15 minutes. Its centre of mass, which moves due to Brownian motion, remains approximately 1µm from the beam core (red cross) at all times.

4.3 Comparison with geometric ray optics model

For particle radii in the range 0.5µm< R_0<5µm, we observe reasonable agreement between the radial force curves predicted by our two models (Fig. 11). Although there are some clear discrepancies in the absolute value of the force predicted by the two models for certain combinations of particle size and radial position (e.g. Fig. 11(b), r=2), for potential sorting

#86741 - $15.00 USD Received 21 Aug 2007; revised 2 Oct 2007; accepted 3 Oct 2007; published 9 Oct 2007

applications the primary concern is the location of stable equilibrium points. For R_0<5µm, the equilibrium points overlap very closely for the two models.

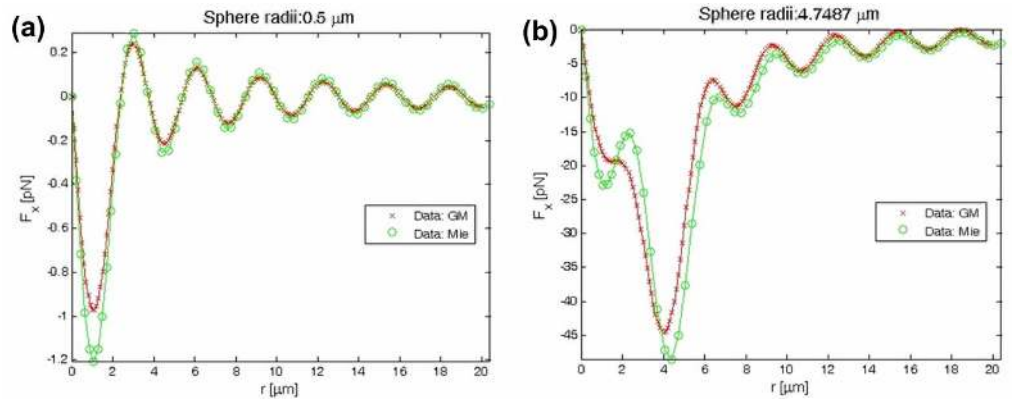

Fig. 11. (Color online) Two comparative plots showing predictions for radial force in a Bessel beam, showing our geometric model (GM) against our Mie model (Mie). (a) R_0=0.5µm. (b) R_0=4.7µm.

As the sphere size increases, the computational effort required to calculate forces using our Mie theory becomes prohibitive. Table 1 provides a comparison between the computation times for our two models. For this test we calculated radial force profiles, similar to those shown in Fig. 11, with 75 radial positions used in each case. These results were obtained on a PC (AMD Athlon 64 X2 Dual 4200+, 2.21 GHz, 2 GB RAM), running Matlab v7.3.0.367 (R2006b) on Windows XP. The time taken for the geometric model to calculate the force profile is independent of particle size. In contrast, the computation time for the Mie model increases exponentially with particle radius.

Table 1. Comparison of Computation Times for Our Two Theoretical Models

Particle radius	R_0=0.5µm	$R_{0=}$5µm	R_0=10µm
Geometric optics model	18.7s	18.7s	18.7s
Mie model	137s	3269s	12893s

To obtain a strong qualitative picture of what underlies optical sorting observed in Bessel beams, it is useful to plot a map of the radial forces experienced by particles as a function of both particle size and radial position in the Bessel beam. In Fig. 12 we present a plot of the predicted force produced using our ray optics model.

#86741 - $15.00 USD Received 21 Aug 2007; revised 2 Oct 2007; accepted 3 Oct 2007; published 9 Oct 2007

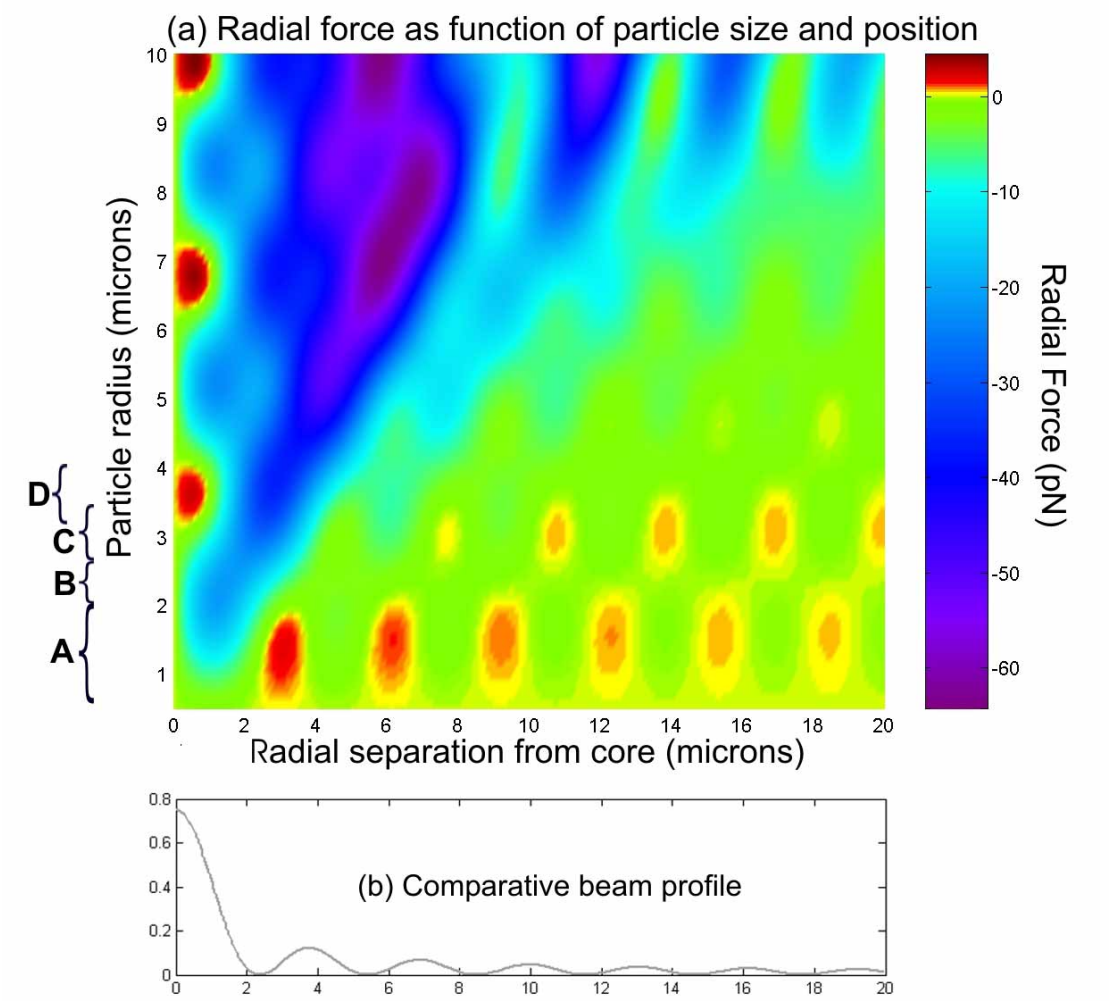

Fig. 12. (Color online) (a) Plot of radial optical force due to a Bessel beam as a function of particle-core separation and particle diameter. (b) Radial intensity profile of Bessel beam for comparison.

Figure 12(a) shows the predicted force plot for a 200mW Bessel beam. A plot of the transverse radial Bessel beam intensity profile is shown in Fig. 12(b) for comparison. The orange-red regions in the force plot correspond to positive radial forces, while the yellow boundaries of these regions identify areas of approximately zero radial force. The yellow regions to the right of the orange-red zones constitute stable equilibrium positions for silica spheres in this Bessel beam.

The hopping regime for particles whose diameter is smaller than or similar to the typical ring spacing can clearly be seen in the bottom right-hand corner of the plot, characterized by a number of regions of alternating positive and negative radial force (zone A). Zone B identifies a narrow region of constant negative radial force. Particles that occupy this regime can be expected to cruise into the core of the Bessel beam without obstruction. As the particle radius is increased further, we see a second zone of oscillating positive and negative radial force emerge (zone C). In contrast to zone A, these regions of positive radial force produce stable equilibrium positions that are spatially matched to the inter-ring intensity minima of the Bessel beam. Zone D overlaps zone C somewhat and is characterized by particle behavior

#86741 - $15.00 USD Received 21 Aug 2007; revised 2 Oct 2007; accepted 3 Oct 2007; published 9 Oct 2007

close to the core of the Bessel beam. Particles that lie within zone D will experience offset core equilibrium positions, as shown in Figs. 5, 6 and 10. As we increase the sphere size further still, both of our models predict that these distinct zones of behavior repeat, although the innermost equilibrium points become increasingly distant from the core with increasing particle radii.

4.4 Static Optical Sorting in a Bessel Beam

The goal of static optical sorting is to spatially separate particles without an applied fluid flow. The response of a dielectric particle to a Bessel beam is strongly dependent on the relationship between its size and the characteristic transverse lengthscales of the Bessel beam. By choosing beam parameters appropriately, it is possible to generate a landscape for which one of the two species will be encouraged to migrate to the core of the beam, while the other remains radially trapped in the beam's rings. With either of our two models, given two suitably distinct particle species we can calculate the parameters of the Bessel required to separate them. Bessel beams can be created using reconfigurable optical devices such as spatial light modulators [30]. As a consequence, this work provides a foundation for the understanding and development of interactive static optical sorting platforms.

5. Conclusion

Using two different theoretical models, we have successfully established a qualitative picture of the physical principles that underlie the previously reported observation of static optical sorting in a Bessel beam [19]. We found that both our Mie and geometrical approaches produced similar predictions for the general nature of the radial optical force, and these have been verified in the laboratory by experiment. In particular, we have elucidated the nature of the locations of stable equilibrium points as a function of particle size, and these results may provide a backdrop to the future development of static optical sorting devices.

Additionally, we made a related observation that builds on earlier work on optical washboard potentials. For particles which are smaller than the typical thickness of the rings that form the Bessel beam (in our case R_0=1.15μm), we observe radial localization in the associated minima of the optical potential. If the beam power is sufficiently low, these particles can thermally escape the radial potential energy wells and *hop* to adjacent rings. Due to slight asymmetries in the local radial intensity profile of any given ring, both of our models predict a relative lowering of the potential energy barrier on the inner side of the ring. As a consequence, small particles are more likely to migrate to the centre of the Bessel beam than away with it, without the need for an explicitly *tilted* Bessel beam as previously suggested [17].

Acknowledgments

We thank the European Science Foundation SONS Programme (grant02-PE-SONS-063-NOMSAN), funded through the UK Engineering and Physical Sciences Research Council (EPSRC) and European Commission 6th Framework Progamme. We also thank the fp6 NEST ADVENTURE programme, through project ATOM3D (no. 508952), for supporting this work. Kishan Dholakia and Karen Volke-Sepulveda acknowledge the support of the Royal Society. Pavel Zemanek acknowledges the support of MEYS through the Centre of Modern Optics (LC06007) and MCT through the project FT-TA2/059. David McGloin is a Royal Society University Research Fellow.

#86741 - $15.00 USD Received 21 Aug 2007; revised 2 Oct 2007; accepted 3 Oct 2007; published 9 Oct 2007